RSC Advances

PAPER

View Article Online
View Journal | View Issue

Cite this: *RSC Adv.*, 2022, **12**, 30174

$NaBiF_4$ upconversion nanoparticle-based electrochemiluminescent biosensor for *E. coli* O157 : H7 detection†

Danqing Liu, *[a] Xingxing Lv,[a] Chaoyue Zhao,[a] Jiayue Li,[a] Jinmei Huang,[a] Ling Weng, *[a] Liangcan He *[b] and Shaoqin Liu [b]

Received 20th August 2022
Accepted 11th October 2022

DOI: 10.1039/d2ra05217b

rsc.li/rsc-advances

Foodborne or water-borne pathogens pose great threats to human beings and animals. There is an urgent need to detect pathogens with cheap, rapid and sensitive point-of-care diagnostic assays. Herein, we report the electrochemiluminescent (ECL) behaviors of $NaBiF_4 : Yb^{3+}/Er^{3+}$ upconversion nanoparticles (UCNPs) which were synthesized *via* a fast and environment-friendly method at room temperature for the first time. The UCNPs together with $K_2S_2O_8$ exhibit high ECL intensity and stable cathodic signals. Further, the Au nanoparticles (Au NPs) and Anti-*E. coli* O157 : H7 antibody were assembled on the surface of UCNPs successively to construct a novel ECL immunosensor for the detection of deadly *E. coli* O157 : H7. The as-prepared ECL immunosensor reveals high sensitivity to *E. coli* O157 : H7 in a linear range of 200–100 000 CFU mL^{-1}, and the minimum detection limit could reach up to 138 CFU mL^{-1}. The designed UCNP-based biosensor demonstrates high specificity, good stability and remarkable repeatability, and the strategy will provide a sensitive and selective method for rapid detection of *E. coli* O157 : H7 in food safety and preclinical diagnosis.

1. Introduction

Foodborne pathogens, such as enterohaemorrhagic *E. coli* with the representative strain of serotype O157 : H7, contaminate food and drinking water posing great threats to human beings and animals.[1,2] The spread of pathogens causes more than 20 000 illnesses and 200 deaths every year in America alone as reported by the CDC. They have been found in more than 20 countries in five states of the world and caused outbreaks and epidemics.[3] For rapid response to disease outbreaks caused by foodborne or water-borne pathogens, it is highly desired to develop novel technologies that can detect pathogens quickly and cheaply anywhere.[4] However, due to the low concentration of bacteria in the actual samples, many traditional methods require multiple procedures such as bacterial culture and enrichment steps in the detection of pathogens, and the pretreatment process is time-consuming.[2] Recently developed detection methods, such as polymerase chain reaction (PCR),[5] surface plasmon resonance (SPR),[6] immunoassay,[7] *etc.*, are much faster; however, these methods either require expensive equipment or are not sensitive enough, which seriously limit their application in the field.

Electrochemiluminescence (ECL) is a kind of electrogenerated chemiluminescence reaction controlled by electrode potential, which has advantages of low cost, high sensitivity, high signal-to-noise ratio and easy controlling. Therefore, it is widely employed in drug and food analysis, preclinical diagnosis, environmental pollutant monitoring, immune detection and other fields.[8] It should be pointed out that the ECL light emitter plays an important role in ECL system. So far, various phosphors, such as ruthenium(II) complexes and luminol developed in early days, and other various nanomaterials, such as precious metal nanoclusters,[9–11] semiconductor quantum dots, graphene quantum dots (GQDs), carbon nanodots have been applied in the ECL system.[12–17] It's a general trend to explore and investigate novel and efficient ECL materials. Rare earth-doped

[a]*School of Material Science and Chemical Engineering, Harbin University of Science and Technology, Harbin 150040, China. E-mail: danqingliu76@163.com; wengling79@163.com*

[b]*Key Laboratory of Micro-systems and Micro-structures Manufacturing of Ministry of Education, Harbin Institute of Technology, Harbin 150001, China. E-mail: liangcanhe@hit.edu.cn*

† Electronic supplementary information (ESI) available: SEM elemental mapping of (B) F, (C) Na, (D) Bi, (E) Yb and (F) Er according to (A) the original SEM image of $NaBiF_4 : Yb^{3+}/Er^{3+}$ UCNPs. XRD pattern of $NaBiF_4 : Yb^{3+}/Er^{3+}$ UCNPs in comparison with the standard peaks of hexagonal phase $NaBiF_4$. Comparison of ECL intensity of $NaBiF_4 : Yb^{3+}/Er^{3+}$ UCNPs in PBS (0.1 M, pH 7.4) with or without 0.1 M $K_2S_2O_8$. Comparison of ECL intensity for different materials with or without doping elements. (A) SEM image and (B) EDS of $NaBiF_4 : Yb^{3+}$ UCNPs, (C) SEM image and (D) EDS of $NaBiF_4$ UCNPs. Effect of the concentration of UCNPs solution on ECL intensity of $NaBiF_4 : Yb^{3+}/Er^{3+}$ UCNPs/GCE. Effect of incubation time on ECL intensity of *E. coli* O157 : H7 antibody/Au/$NaBiF_4 : Yb^{3+}/Er^{3+}$ UCNPs/GCE. The relationship between the ECL peak intensity and the logarithm of *E. coli* Top 10 concentrations with the anti-*E. coli* O157 : H7/Au/$NaBiF_4 : Yb^{3+}/Er^{3+}$ UCNPs/GCE incubated with *E. coli* top 10. The long-time stability of as-prepared biosensors. The selectivity and specificity of the biosensor. See DOI: https://doi.org/10.1039/d2ra05217b

UCNPs could absorb two or more low-energy photons and emit high-energy photons, and possess the advantages of good biocompatibility, good emission stability, less photobleaching and deeper tissue penetration. So, they are widely used in biomedical fields such as bioanalysis and *in vivo* imaging.[18,19] As a promising luminescent material, UCNPs have been developed as the next-generation of ECL luminescent reagents in recent years, which have a series of potential advantages, such as stable cathodic signal, high luminous intensity, ideal ECL emission signal and long fluorescence lifetime.[20] Generally speaking, there are few reports about the applications of UCNPs in ECL field. For example, Qu Group successfully developed reduced graphene oxide-$NaYF_4$: Yb/Er hybrid nanomaterials (rGO-UCNPs) with amplified ECL performance.[21,22] Liu *et al.*[23] and Guo *et al.*[24] reported the Mn^{2+}-doped $NaYF_4$: Yb/Er UCNPs which were used for tumor biomarker and bisphenol A detection, respectively. Recently, Wang group developed molecularly imprinted ECL biosensors based on SiO_2–NH_2 modified $NaYF_4$: Yb/Tm and $NaYF_4$: Yb/Er UCNPs.[25,26] Up to now most of the reported UCNPs matrix used in the ECL detection are $NaYF_4$.[27] However, the $NaYF_4$ process is complex, high cost and easy to cause environmental problems, severely limiting its further application in ECL. Therefore, it is of great significance to develop a fast and environment-friendly synthesis method. Alternatively, the $NaBiF_4$-type hexagonal UCNPs can be synthesized at room temperature under mild conditions, and moreover bismuth ion is environmentally friendly. The $NaBiF_4$-type UCNPs, a potential ECL luminophore, is expected to replace $NaYF_4$-type UCNPs.

Herein, a novel effective ECL biosensor based on $NaBiF_4$ UCNPs is proposed for pathogens inspection, which exhibits rapid response, high ECL intensity, and excellent stability. In this work, the *E. coli* O157 : H7 antibody was conjugated with Au/$NaBiF_4$ *via* antibody–Au interaction, and thus an effective ECL biosensor was fabricated for *E. coli* O157 : H7 detection. In the presence of *E. coli* O157 : H7, the ECL emission from the immunosensor would be largely inhibited due to the existence of non-conductive biological complex. Moreover, our experimental results reveal that the ECL biosensor has high sensitivity and wide detection range (200–100 000 CFU mL^{-1}) with a very low detection limit of 138 CFU mL^{-1} for *E. coli* O157 : H7 detection. The high specificity, remarkable repeatability and good stability would provide a facile strategy for *E. coli* O157 : H7 detection in food safety and preclinical diagnosis.

2. Experimental

2.1 Materials

Chloroauric acid ($HAuCl_4$) and bovine serum albumin (BSA, 96–99% purity) were purchased from Sigma-Aldrich company. $NaNO_3$, NH_4F, $Yb(NO_3)_3 \cdot 5H_2O$, $Er(NO_3)_3 \cdot 5H_2O$, $Bi(NO_3)_3 \cdot 5H_2O$ and other chemicals were bought from Aladdin company. The deionized water (18.2 MΩ) was generated by a Milli-Q Millipore purifier. The *E. coli* O157 : H7 strain (ATCC number 43889) and *E. coli* O157 : H7 polyclonal antibody were bought from Prajna Biology Company, Shanghai.

2.2 Apparatus

The morphology of the materials was characterized by a field emission scanning electron microscope (FESEM, FEI Quanta 200F). The crystal structure of the sample was investigated by an X-ray powder diffraction (Empyrean, Malvern Panalytical instruments) equipped with Cu Ka radiation ($\lambda = 0.154184$ nm) ranging from 20° to 80°. The upconversion luminescence spectra were recorded by a luminescence spectrophotometer (F-7000, Hitachi Co., Japan) with an 980 nm laser (Hi-Tech Optoelectronic Co., China). Chenhua CHI 860D electrochemistry workstation was used for the measurement of cyclic voltammetry (CV) and offered the external potential for the measurement of ECL spectra related to wavelength, along with a luminescence spectrophotometer (LS55, PerkinElmer, USA). Electrochemical impedance spectra (EIS) were measured on an Autolab potentiostat (PGSTAT320N, Switzerland) with wide frequency range (0.1 to 100 KHz) in 5 mM $[Fe(CN)_6]^{4-/3-}$ solution (10 mM PBS, pH 7.4) and plotted in the form of Nyquist plots. ECL emission was tested by an MPI-A ECL tester (Xi'An Remax Electronic Science & Technology, China). A conventional 3-electrode system was utilized in all the above electrochemical measurements, which was comprised of a glassy carbon working electrode (GCE, $\Phi = 3$ mm) modified with $NaBiF_4$: Yb^{3+}/Er^{3+} UCNPs, reference electrode (Ag/AgCl) and a platinum wire auxiliary electrode, respectively.

2.3 Synthesis of the $NaBiF_4$: Yb^{3+}/Er^{3+} UCNPs

The $NaBiF_4$: Yb^{3+}/Er^{3+} UCNPs were prepared based on previously reported literature.[28] The clear and transparent solution 1 was prepared by dissolving $NaNO_3$(2 mmol), $Yb(NO_3)_3 \cdot 5H_2O$ (0.2 mmol), $Bi(NO_3)_3 \cdot 5H_2O$ (0.78 mmol), and $Er(NO_3)_3 \cdot 5H_2O$ (0.02 mmol) in 10 mL ethylene glycol (EG) solution. Solution 2 was prepared by adding NH_4F (14 mmol) to 25 mL EG solution. Then, the solution 1 was slowly dripped into solution 2 with vigorous stirring and reacted for 10 minutes at room temperature along with violently magnetic stirring to get a white emulsion. After several times of centrifugation, the white powder was obtained by vacuum drying at 60 °C for further use. The preparation of $NaBiF_4$ or $NaBiF_4$: Yb^{3+} NPs as the control materials is same as that of $NaBiF_4$: Yb^{3+}/Er^{3+} UCNPs, only without $Yb(NO_3)_3 \cdot 5H_2O$ and $Er(NO_3)_3 \cdot 5H_2O$ for $NaBiF_4$ NPs and without $Er(NO_3)_3 \cdot 5H_2O$ for $NaBiF_4$: Yb^{3+} NPs.

2.4 Fabrication of the ECL immunsensors

A certain amount of as-prepared UCNPs is dispersed into a mixed solution containing Nafion, isopropanol and water (volume ratio is 2 : 49 : 49) at 0.5 mg mL^{-1}. The bare glassy carbon electrode was continuously polished with aluminum oxide paste (1.0, 0.3 and 0.05 μm) to make its surface smooth, then washed with deionized water. Subsequently, cyclic voltammetry was tested in 1 mmol L^{-1} K_3 $[Fe(CN)_6]$ (including 0.2 mol L^{-1} KNO_3) until the peak potential difference was less than 80 mV. Then, 10 μL UCNPs solution (0.5 mg mL^{-1}) was dripped onto the surface of GCE electrode, and the UCNPs modified

electrode (UCNPs/GCE) was obtained after drying at room temperature.

After that, 10 μL Au NPs solution[29] was dropped onto the surface of UCNPs/GCE, and 10 μL anti-*E. coli* O157 : H7 polyclonal antibody (10 μg mL^{-1}, 0.1 M PBS, pH 7.4) was incubated on the film overnight at 4 °C. After washing with PBS, the antibody modified electrode was incubated with BSA solution (1%, w/w) for 1 hour to block the nonspecific sites. The as-prepared immunosensors were then stored at 4 °C for further use.

2.5 ECL detection of *E. coli* O157 : H7

Typically, a fixed volume of *E. coli* O157 : H7 (10 μL) with various concentration (0 to 500 000 CFU ml^{-1}) was incubated with as-prepared biosensors (37 °C for 40 min) respectively, in order to immobilize bacteria on the surface of the immunosensors. After being rinsed carefully with PBS solution to remove the non-captured bacteria, the biosensors were used for ECL detection. The ECL signals were detected in 0.1 M PBS containing 0.1 M $K_2S_2O_8$ (pH 7.4) electrolyte solution. The scanning potential ranged from −2.5–0 V at 100 mV s^{-1}. The photomultiplier tube (PMT) voltage was 800 V.

3. Results and discussion

3.1 Characterization of $NaBiF_4 : Yb^{3+}/Er^{3+}$ UCNPs

The $NaBiF_4 : Yb^{3+}/Er^{3+}$ UCNPs were synthesized at room temperature. Then, a series of characterization of $NaBiF_4 : Yb^{3+}/Er^{3+}$ UCNPs were carried out, including SEM morphology characterization, elemental mapping analysis, X-ray diffraction pattern (XRD) and upconversion fluorescence spectrum. It was observed from SEM that the prepared $NaBiF_4 : Yb^{3+}/Er^{3+}$ UCNPs were monodisperse with an average particle size of 228 ± 17 nm (Fig. 1A). The element composition of $NaBiF_4 : Yb^{3+}/Er^{3+}$ UCNPs was confirmed by elemental mapping analysis, and the distribution of all elements was uniform as shown in Fig. S1.† The existence of element Yb and Er directly proved the successful doping of the dopants in $NaBiF_4 : Yb^{3+}/Er^{3+}$ UCNPs. Due to the small amount of Er^{3+} doping in the system, the distribution of elements in the elemental mapping image was sparse.

XRD technique was used to characterize the crystal structure of $NaBiF_4 : Yb^{3+}/Er^{3+}$ UCNPs. As shown in Fig. S2,† the XRD spectra of the as-prepared samples presented its main characteristic diffraction peaks at $2\theta = 28.5°$, 42°and 52°corresponding to the (101), (201) and (211) crystal planes of $NaBiF_4 : Yb^{3+}/Er^{3+}$ UCNPs, which were consistent with the standard hexagonal phase $NaBiF_4 : Yb^{3+}/Er^{3+}$ UCNPs (JCPDS 41-0796). There were no diffraction peaks of other impurities, which confirmed that we had obtained $NaBiF_4$ with hexagonal crystal structure. The diffraction peak of Er^{3+} is generally indistinguishable, mainly due to the low content of doped Er^{3+} (Er is only 2%). Combined with the elemental mapping results, it is confirmed that pure phase $NaBiF_4 : Yb^{3+}/Er^{3+}$ UCNPs were successfully synthesized by this simple method.

ECL behaviour of the $NaBiF_4 : Yb^{3+}/Er^{3+}$-coated GCE electrode was also studied in 0.1 MPBS solution (pH 7.4) with 0.1 M $K_2S_2O_8$ as coreactant. As shown in Fig. 1B, $NaBiF_4 : Yb^{3+}/Er^{3+}$ UCNPs showed a strong ECL emission at −2.5 V at the potential of −2.5–0 V, with an onset potential at about −1.3 V. Moreover, the comparison of the cyclic voltammograms (CVs) between bare GCE with or without $K_2S_2O_8$ in the inset of Fig. 1B showed that a stable reduction peak around about −0.8 V with $K_2S_2O_8$, which confirmed the contribution of the coreactant $S_2O_8^{2-}$ at −0.8 V.[30] The CV of GCE modified with UCNPs showed another reduction peak at about −2.0 V, which could be ascribed to the reduction of $NaBiF_4 : Yb^{3+}/Er^{3+}$ UCNPs. Besides it, the CV of UCNPs/GCE with $K_2S_2O_8$ showed a reduction peak at about −1.0 V. There was a slight deviation compared with the reduction peak of $S_2O_8^{2-}$ at bare GCE with $K_2S_2O_8$, which might be due to the interaction between $S_2O_8^{2-}$ and $NaBiF_4 : Yb^{3+}/Er^{3+}$ UCNPs. As shown in the inset of Fig. 1B, the CV curves of $K_2S_2O_8$, $K_2S_2O_8$\UCNPs and UCNPs showed an onset reduction potential at −0.4 V, −0.7 V and −1.7 V, respectively, suggesting that the interaction between $S_2O_8^{2-}$ and UCNPs effectively changed the onset reduction potential and made it more easily to be reduced.[31] The onset potential of ECL spectrum was recorded at −1.3 V with a peak wavelength of about 530 nm, ascribing to the ECL emission of UCNPs combined with $K_2S_2O_8$ (Fig. 1B and C). ECL intensity of UCNPs with $K_2S_2O_8$ was about 4-fold as that of UCNPs without $K_2S_2O_8$ (Fig. S3†). This indicated that the strong ECL signal was generated only after the reduction of both UCNPs and $K_2S_2O_8$.

The upconversion fluorescence spectrum of $NaBiF_4 : Yb^{3+}/Er^{3+}$ UCNPs was measured using the 980 nm laser. The result is shown in the inset of Fig. 1C. The upconversion fluorescence emission spectrum includes green emission spectrum of 510–565 nm and red emission spectrum of 630–690 nm. Among them, the green emission peak comes from $^2H_{11/2}$ to $^4I_{15/2}$ transition and $^4S_{3/2}$ to $^4I_{15/2}$ transition of the Er^{3+} ion, and the red emission peak comes from $^4F_{9/2}$ to $^4I_{15/2}$ transition of the Er^{3+} ion. ECL spectrum of $NaBiF_4 : Yb^{3+}/Er^{3+}$ UCNPs achieving maximum at about 530 nm presented a relatively wide ECL signal, which is consistent with the green emission part from 510 to 565 nm in upconversion fluorescence spectrum (see Fig. 1C). To explore the role of doping elements in ECL, more control studies were carried out. The synthesized control materials without doping elements of Er or both Er and Yb were confirmed by EDS and the morphology of particles slightly collapsed with the missing of both doping elements (Fig. S4†). The ECL intensity was decreased dramatically with the missing of doping elements indicating the important role of doping elements in ECL process (Table S1†).

For ECL process, electron first injected into UCNPs under the negative potential and then the $NaBiF_4 : Yb, Er$ was reduced to negatively charged radical ($NaBiF_4 : Yb, Er^{-\bullet}$). At the meantime, the coreactant $S_2O_8^{2-}$ was electrochemically reduced to the strong oxidant-anion sulfate radical ($SO_4^{-\bullet}$) and further reacted with $NaBiF_4 : Yb, Er^{-\bullet}$ to produce excited state $NaBiF_4 : Yb, Er^*$. Subsequently, $NaBiF_4 : Yb, Er^*$ returned to ground state and released photons, resulting in a strong ECL signal. The ECL mechanism of $NaBiF_4 : Yb, Er$ UCNPs shown in Fig. 1D was suggested as follows based on oxidation-reduction (Ox-red) pathway:[32]

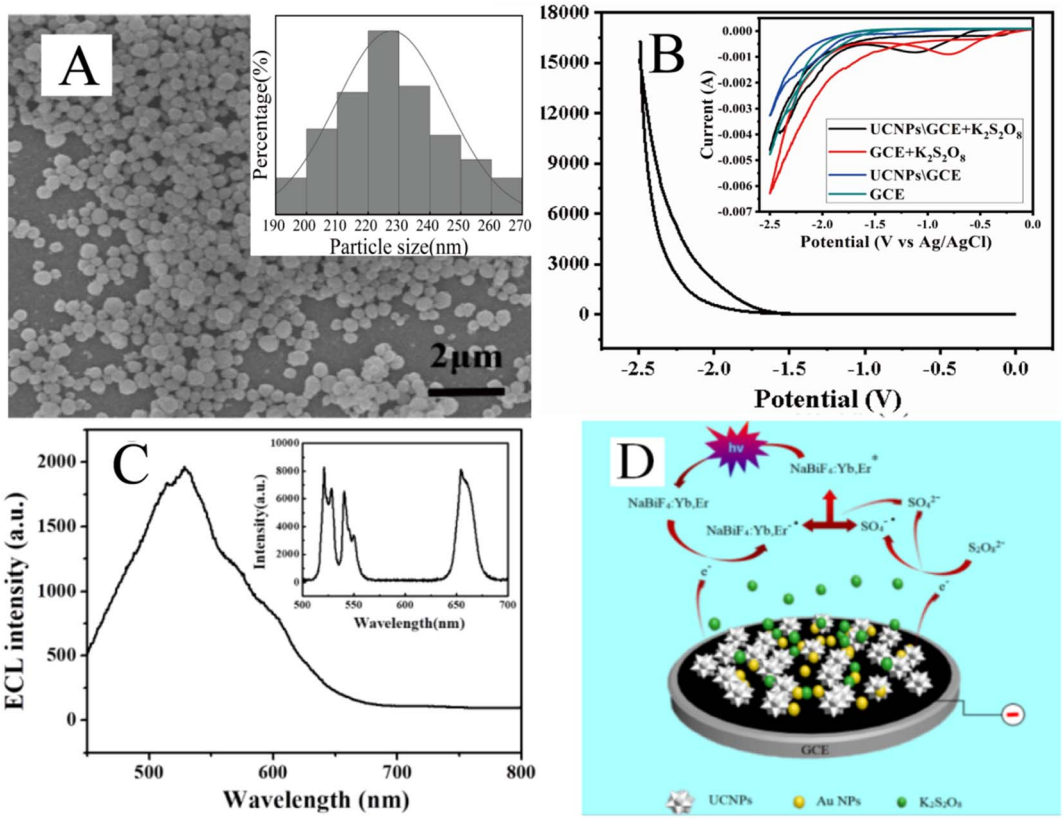

Fig. 1 (A) SEM image and the particle size distribution (inset) of $NaBiF_4:Yb^{3+}/Er^{3+}$ UCNPs. (B) ECL-potential curve of $NaBiF_4:Yb^{3+}/Er^{3+}$ UCNPs/GCE in 0.1 M PBS (pH 7.4) containing 0.1 M $K_2S_2O_8$ with the scan rate of 100 mV s^{-1} and the PMT voltage of 800 V. The inset shows cyclic voltammogram of bare GCE with or without $K_2S_2O_8$ and $NaBiF_4:Yb^{3+}/Er^{3+}$ UCNPs/GCE with or without $K_2S_2O_8$ in 0.1 M PBS (pH 7.4). The scan rate was 50 mV s^{-1}. (C) ECL spectrum of $NaBiF_4:Yb^{3+}/Er^{3+}$ UCNPs/GCE in 0.1 M PBS (pH 7.4) containing 0.1 M $K_2S_2O_8$, under the potential of −2.5 V and upconversion fluorescence spectrum (inset) of $NaBiF_4:Yb^{3+}/Er^{3+}$ UCNPs. (D) ECL mechanism of the $NaBiF_4:Yb^{3+}/Er^{3+}$ UCNPs.

$$NaBiF_4:Yb,Er + e^- \rightarrow NaBiF_4:Yb,Er^{-\bullet} \quad (1)$$

$$S_2O_8^{2-} + e^- \rightarrow SO_4^{2-} + SO_4^{-\bullet} \quad (2)$$

$$NaBiF_4:Yb,Er^{-\bullet} + SO_4^{-\bullet} \rightarrow NaBiF_4:Yb,Er^* + SO_4^{2-} \quad (3)$$

$$NaBiF_4:Yb,Er^* \rightarrow NaBiF_4:Yb,Er + h\nu \quad (4)$$

3.2 Characterization and fabrication of the ECL biosensor

The high ECL intensity of $NaBiF_4:Yb^{3+}/Er^{3+}$ UCNPs shows the potential application in ECL biosensor. Each fabrication process of the immunosensor could be characterized by the electrochemical impedance spectra (EIS). Fig. 2A shows the Nyquist plots of impedance spectra recorded after each fabrication process in 0.1 M PBS containing 5 mM $[Fe(CN)_6]^{3-/4-}$ and 0.1 M KCl. The inset of Fig. 2A is the circuit diagram for the fitting process, where R_s represents the solution resistance, R_{ct} represents the resistance of the contact interface between the working electrode and the solution, Q represents the capacitance caused by the double electric layer at the contact interface between the working electrode and the solution, and W represents the diffusion impedance according to the Warburg Weber diffusion. The semicircle diameter of the EIS Nyquist plots represents the charge transfer resistance (R_{ct}) value at the liquid–solid interface. The bare GCE displayed a small semicircle domain with R_{ct} value of 227 Ω (Fig. 2A, curve a). When bare GCE was modified with $NaBiF_4:Yb^{3+}/Er^{3+}$ UCNPs, the impedance increased to a higher R_{ct} value of 703 Ω (Fig. 2A, curve b), indicating that the UCNPs material restrained electron transfer from the electroactive probe. After Au nanoparticles were assembled on the electrode surface of $NaBiF_4:Yb^{3+}/Er^{3+}$ UCNPs, an obvious decrease of R_{ct} value to 73 Ω was observed because the Au NPs have excellent electrical conductivity and accelerate electron transfer between interfaces (Fig. 2A, curve c). The impedance obviously increased to 4273 Ω when the antibodies of *E. coli* O157 : H7 functionalized on Au NPs/UCNPs/GCE modified electrode (Fig. 2A, curve d), since the insulting protein layer could disturb the electron transfer between the electrode and $K_3Fe(CN)_6$. After the antibody/Au NPs/UCNPs/GCE was incubated with *E. coli* O157 : H7 (1000 CFU mL^{-1}), the impedance significantly increased to 9500 Ω because of the attachment of bacteria (Fig. 2A, curve e).

The fabrication steps of ECL biosensor were also confirmed by the change of ECL signals during the gradual modification process with materials and biomolecules. As shown in Fig. 2B, there had weak ECL intensity for bare GCE (curve a). While, the

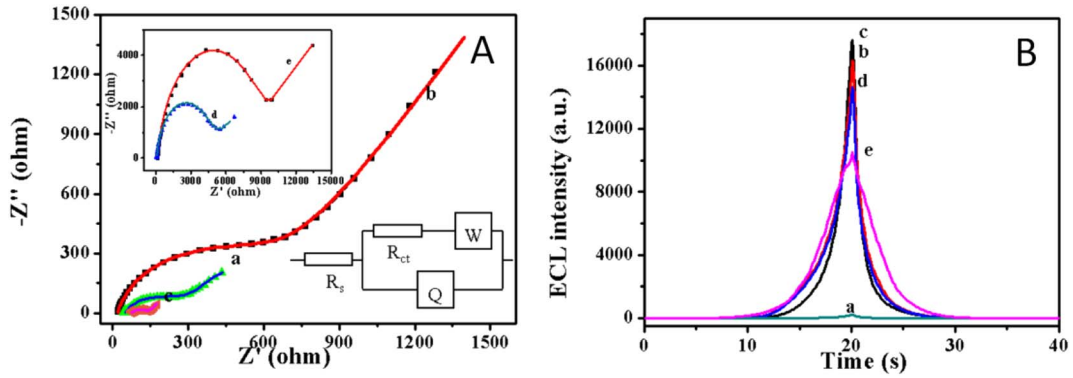

Fig. 2 (A) Electrochemical impedance Nyquist plots of (a) bare GCE electrode, (b) $NaBiF_4:Yb^{3+}/Er^{3+}$ UCNPs/GCE, (c) Au NPs/$NaBiF_4:Yb^{3+}/Er^{3+}$ UCNPs/GCE, (d) antibody/Au NPs/$NaBiF_4:Yb^{3+}/Er^{3+}$ UCNPs/GCE and (e) *E. coli* O157 : H7/antibody/Au NPs/$NaBiF_4:Yb^{3+}/Er^{3+}$ modified glassy carbon electrodes in PBS solution (10 mM, pH 7.4, containing 5 mM $[Fe(CN)_6]^{3-/4-}$), the frequency ranged from 0.1 Hz to 100 kHz with the amplitude of 5 mV. (B) ECL-time curves of (a) bare GCE electrode, (b) $NaBiF_4:Yb^{3+}/Er^{3+}$ UCNPs/GCE, (c) Au NPs/$NaBiF_4:Yb^{3+}/Er^{3+}$ UCNPs/GCE, (d) antibody/Au NPs/$NaBiF_4:Yb^{3+}/Er^{3+}$ UCNPs/GCE and (e) *E. coli* O157 : H7/antibody/Au NPs/$NaBiF_4:Yb^{3+}/Er^{3+}$ UCNPs modified glassy carbon electrodes in PBS (0.1 M, pH 7.4, containing 0.1 M $K_2S_2O_8$) solution (scan rate: 100 mV s^{-1}; PMT voltage: 800 V).

$NaBiF_4:Yb^{3+}/Er^{3+}$ UCNPs was successfully modified on GCE surface, the ECL intensity increased up to ~16 250 a. u. (curve b). Moreover, further enhancement of ECL intensity was observed after the deposition of Au NPs (17 618 a. u., curve c) since Au NPs could improve the conductivity of modified electrode and thus facilitate the charge transfer of $NaBiF_4:Yb^{3+}/Er^{3+}$ in the ECL reaction.[33] The intensity of ECL decreased to ~14 600 a. u. (curve d) quickly when anti-*E. coli* O157 : H7 antibody was immobilized on the electrode surface *via* the strong interaction with amine groups of Au NPs, revealing that the electron transfer kinetics resistance of protein membranes reduced the diffusion rate of ECL reagent at the electrode interface. After 3000 CFU mL^{-1} *E. coli* O157 : H7 successfully immobilized on the biosensor *via* antigen–antibody binding force, the ECL intensity also dramatically decreased. All the above results clearly indicated the successful fabrication of the biosensor.

The AuNPs/$NaBiF_4:Yb^{3+}/Er^{3+}$ UCNPs functionalized glassy carbon electrode was scanned for 20 cycles continuously under the negative potential ranging from −2.5 to 0 V and the ECL signals had no obvious decrease (see Fig. 3). Thus, the as-prepared ECL biosensor exhibited an excellent stability and would be a promising candidate for further ECL detection.

3.3 Condition optimization and detection of *E. coli* O157 : H7

In order to study the optimal ECL performance, the effects of incubation time and the concentration of UCNPs solution on ECL signal were investigated. The effects of the concentration of UCNPs solution on ECL signal are shown in Fig. S5.† The ECL intensity increased with the increasing of solution concentrations from 0.1 to 0.5 mg mL^{-1}, and then decreased when the UCNPs solution concentration was greater than 0.5 mg mL^{-1}. Thus, the UCNPs solution (0.5 mg mL^{-1}) was selected for preparation of the biosensor. For the incubation time, the prepared sensors were exposed to 10 000 CFU mL^{-1} *E. coli* O157 : H7 suspension solution for different time to investigate the effect of incubation time on ECL signal (Fig. S6†). The ECL signals firstly decreased within the incubation time of 0–45 min, then started to level off at 45–60 min, indicating the saturation status of the amount of *E. coli* O157 : H7 assembled on the electrode surface. Therefore, 45 min is chosen in the following experiments.

Then, the relationship between *E. coli* O157 : H7 and the ECL intensity were investigated under the optimized conditions. The bacteria concentration-ECL response and the calibration curve shown in Fig. 4A and B evidently indicated that the ECL intensity decreased gradually with increasing bacteria concentrations, and was proportional to the bacteria concentrations within 200–100000 CFU mL^{-1}. While, when the concentration of *E. coli* O157 : H7 reached up to 100 000 CFU mL^{-1}, the decrease of the ECL intensity of the sensor flattened out since all binding sites were occupied by *E. coli* O157 : H7. Fig. 4B depicted that the linear range for *E. coli* O157 : H7 detection was from 200–100000

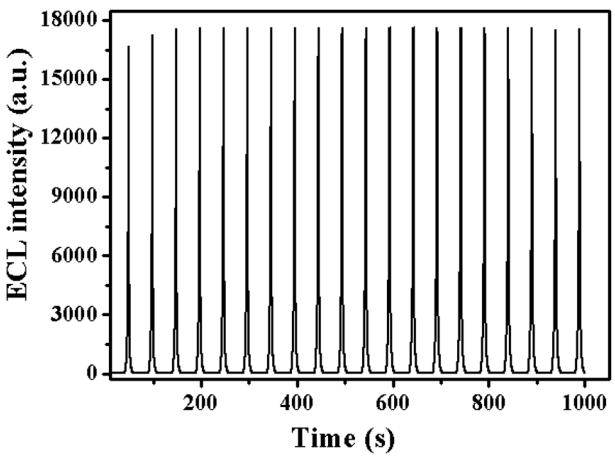

Fig. 3 ECL emission from the AuNPs/$NaBiF_4:Yb^{3+}/Er^{3+}$ UCNPs/GCE electrode in 0.1 M PBS (pH 7.4) containing 0.1 M $K_2S_2O_8$ under continuous cyclic voltammetry for 20 cycles (scan rate: 100 mV s^{-1}; PMT voltage: 800 V).

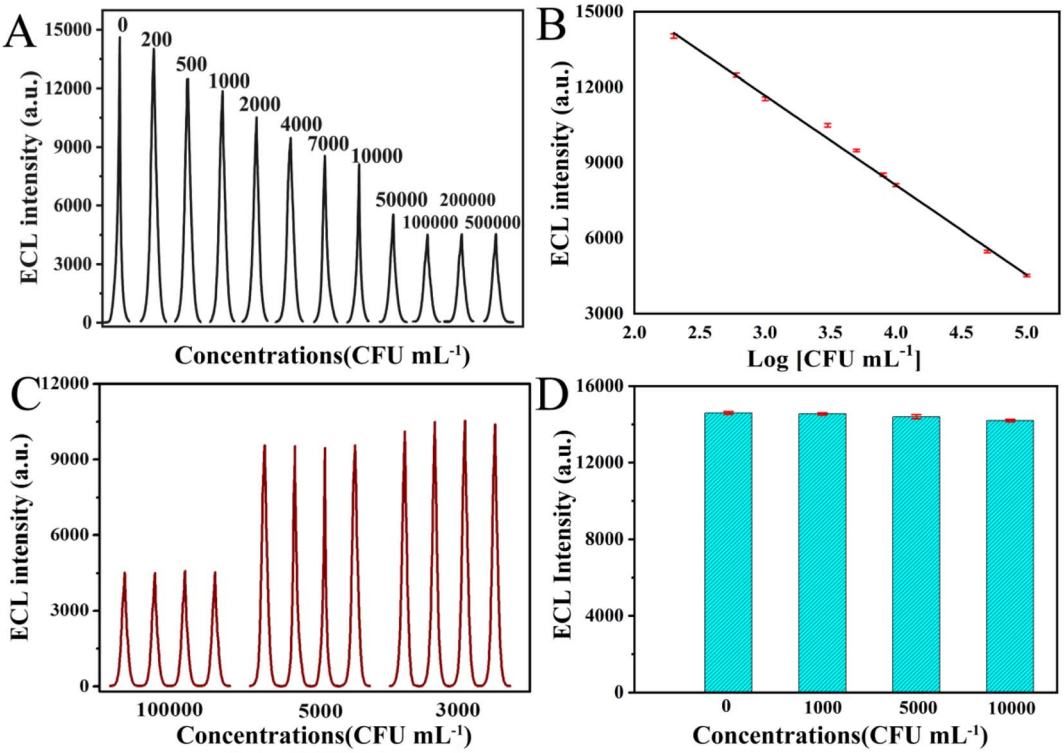

Fig. 4 (A) ECL response curves of the anti- *E. coli* O157 : H7/Au/$NaBiF_4$: Yb^{3+}/Er^{3+} UCNPs modified glassy carbon electrode after incubated with *E. coli* O157 : H7 (0, 200, 600, 1000, 3000, 5000, 8000, 10 000, 50 000, 100 000, 200 000 and 500 000 CFU mL^{-1}). (B) The calibration curve for ECL sensor. (Error bar: RSD, $n = 5$). (C) The immunosensor reproducibility in the detection of *E. coli* O157 : H7 (3000, 5000 and 100 000 CFU mL^{-1}). (D) The immunosensor selectivity in the detection of *E. coli* Top10.

CFU mL^{-1} (correlation coefficient: 0.995). The regression equation was $I_{ECL} = 22\,645.8–3621.7 \log(C_{bacteria})$, where I_{ECL} and $C_{bacteria}$ represents the ECL intensity, and the concentration of *E. coli* O157 : H7, respectively. Based on IUPAC standard, the detection limit was calculated to be 138 CFU mL^{-1}.

In order to evaluate the reproducibility of as-prepared biosensor, 4 successive assays were measured to detect *E. coli* O157 : H7 at various concentrations (3000, 5000 and 100 000 CFU mL^{-1}, Fig. 4C). The RSD was 2.2%, 1.5% and 0.8%, respectively, indicating its good reproducibility. The stability of the immunosensor was further investigated. After stored for 2 weeks at 4 °C, the ECL intensity of stored biosensors still remained about 93.5% of the initial intensity, demonstrating good long-time stability (see Table S2†).

The biosensor selectivity and specificity were later investigated. *E. coli* Top 10 was used as a contrast in the selectivity evaluation of the developed biosensor for *E. coli* O157 : H7, because there has no O157 and H7 antigen. As shown in Fig. 4D, the sensor showed almost no obvious ECL response to non-specific bacteria strain and no apparent ECL intensity change for *E. coli* Top 10 at different concentrations (1000 to 10 000 CFU mL^{-1}). With the further increase of the concentrations in the range of 10 000–500 000 CFU mL^{-1}, there has slight decrease of ECL intensity for *E. coli* top 10 due to the physical adhesion (see Fig. S7†). Further investigation was performed to prove the specificity and selectivity of the as-prepared biosensor, which was exposed to the multiple bacteria solution containing *E. coli* O157 : H7, *E. coli* JM109, *E. coli* DH5α and *E. coli* Top 10 with the same concentration of 1000 CFU mL^{-1}. The ECL intensity for multiple bacteria was quite close to the blank experiment for only 1000 CFU mL^{-1} *E. coli* O157 : H7 (see Table S3†).

To further confirm the role of *E. coli* O157 : H7 antibody for the selectivity and specificity of the biosensor, the sensors without *E. coli* O157 : H7 antibody modification were incubated with 10 000 CFU mL^{-1} *E. coli* O157 : H7 and *E. coli* top 10, respectively. The ECL responses of the above biosensors were tested. No obvious changes in the ECL intensity were observed for either *E. coli* O157 : H7 or *E. coli* top 10. The RSD of ECL signals were only 4.6% and 4.8%, respectively, in comparison with the blank experiment (see Table S3†). So, the strong antigen–antibody binding affinity evidently proved the important role in capturing *E. coli* O157 : H7. Such good performance indicated that the antibody functionalized UCNPs-based biosensor possessed good binding selectivity, excellent stability and strong ECL emission, thus had great potential in facile detection of *E. coli* O157 : H7.

4. Conclusions

The $NaBiF_4$: Yb^{3+}/Er^{3+}UCNPs were successfully synthesized by a fast and environment-friendly method at room temperature, which was further utilized for the preparation ECL immunosensor in *E. coli* O157 : H7 detection for the first time. The UCNPs exhibit high ECL intensity and stable cathodic signals in

the presence of $K_2S_2O_8$. The ECL immunosensor modified with Anti-*E. coli* O157 : H7 antibody/Au NPs/UCNPs exhibited remarkable selectivity, repeatability and operational stability for the detection of *E. coli* O157 : H7. A linear detection scope from 200 to 100 000 CFU mL^{-1} and a low detection limit of 138 CFU mL^{-1} for *E. coli* O157 : H7 have been obtained by using such novel ECL immunosensor. In this work, cheap and environment-friendly $NaBiF_4$-type hexagonal UCNPs are expected to become a potential novel ECL luminophore and could be further utilized for the detection of other biomolecules such as cancer biomarkers, demonstrating a promising nanoplatform in food safety and disease diagnostics.

Author contributions

Danqing Liu: conceptualization, methodology, investigation, writing-original draft, review & editing, funding acquisition. Xingxing Lv: methodology, data curation. Chaoyue Zhao: visualization, software. Jiayue Li: software, investigation. Jinmei Huang: methodology and investigation. Ling Weng: project administration, writing-reviewing and editing. Liangcan He: supervision, writing-reviewing and editing. Shaoqin Liu: supervision, funding acquisition.

Conflicts of interest

The authors declare that they have no known competing financial interests or personal relationships that could have appeared to influence the work reported in this paper.

Acknowledgements

We would like to appreciate the financial support from the National Natural Science Foundation of China (no. 52172085), and Key Laboratory of Micro-systems and Micro-structures Manufacturing (Harbin Institute of Technology), Ministry of Education (no. 2020KM007).

References

1 L. Varadi, J. L. Luo, D. E. Hibbs, J. D. Perry, R. J. Anderson, S. Orenga and P. W. Groundwater, *Chem. Soc. Rev.*, 2017, **46**, 4818–4832.
2 A. Rompre, P. Servais, J. Baudart, M. R. de-Roubin and P. Laurent, *J. Microbiol. Methods*, 2002, **49**, 31–54.
3 P. D. Frenzen, A. Drake, F. J. Angulo and Emerging Infections Program, *J. Food Prot.*, 2005, **68**, 2623–2630.
4 E. Cesewski and B. N. Johnson, *Biosens. Bioelectron.*, 2020, **159**, 112214.
5 J. M. Caldwell, in *Annual Review of Food Science and Technology*, ed. M. P. Doyle and T. R. Klaenhammer, 2017, vol. 8, pp. 57–74.
6 S.-Y. Kwak, M. H. Wong, T. T. S. Lew, G. Bisker, M. A. Lee, A. Kaplan, J. Dong, A. T. Liu, V. B. Koman, R. Sinclair, C. Hamann and M. S. Strano, in *Annual Review of Analytical Chemistry*, ed. R. G. Cooks and J. E. Pemberton, 2017, vol. 10, pp. 113–140.
7 I.-H. Cho, A. D. Radadia, K. Farrokhzad, E. Ximenes, E. Bae, A. K. Singh, H. Oliver, M. Ladisch, A. Bhunia, B. Applegate, L. Mauer, R. Bashir and J. Irudayaraj, in *Annual Review of Analytical Chemistry*, 2014, vol. 7, pp. 65–88.
8 Z. H. Qiao, Y. C. Fu, C. Y. Lei and Y. B. Li, *Food Control*, 2020, **112**, 107116.
9 C. Han and W. Guo, *Small*, 2020, e2002621, DOI: **10.1002/smll.202002621**.
10 M.-C. Pan, Y.-M. Lei, Y.-Q. Chai, R. Yuan and Y. Zhuo, *Anal. Chem.*, 2020, **92**, 13581–13587.
11 L. Zhu, J. Ye, M. Yan, Q. Zhu, S. Wang, J. Huang and X. Yang, *ACS Sens.*, 2019, **4**, 2778–2785.
12 L. Hu, Y. Wu, M. Xu, W. Gu and C. Zhu, *Chem. Commun.*, 2020, **56**, 10989–10999.
13 J. R. Adsetts, R. Zhang, L. Yang, K. Chu, J. M. Wong, D. A. Love and Z. Ding, *Front. Chem.*, 2020, **8**, 580022.
14 Y. Chen, Y. Cao, C. Ma and J.-J. Zhu, *Mater. Chem. Front.*, 2020, **4**, 369–385.
15 Q. Zhai, J. Li and E. Wang, *Chemelectrochem*, 2017, **4**, 1639–1650.
16 X. Chen, Y. Liu and Q. Ma, *J. Mater. Chem. C*, 2018, **6**, 942–959.
17 F. C. Cui, Y. L. Ye, J. F. Ping and X. L. Sun, *Biosens. Bioelectron.*, 2020, **156**, 112085.
18 R. Rafique, S. K. Kailasa and T. J. Park, *TrAC, Trends Anal. Chem.*, 2019, **120**, 115646.
19 H. Li, X. Wang, D. Huang and G. Chen, *Nanotechnology*, 2020, **31**, 072001.
20 J. Zhou, Z. Liu and F. Li, *Chem. Soc. Rev.*, 2012, **41**, 1323–1349.
21 M. Yin, L. Wu, Z. Li, J. Ren and X. Qu, *Nanoscale*, 2012, **4**, 400–404.
22 L. Wu, J. Wang, M. Yin, J. Ren, D. Miyoshi, N. Sugimoto and X. Qu, *Small*, 2014, **10**, 330–336.
23 M. Liu, Y. Ye, C. Yao, W. Zhao and X. Huang, *J. Mater. Chem. C*, 2014, **2**, 6626–6633.
24 X. Guo, S. Wu, N. Duan and Z. Wang, *Anal. Bioanal. Chem.*, 2016, **408**, 3823–3831.
25 Y. Gu, J. Wang, H. Shi, M. Pan, B. Liu, G. Fang and S. Wang, *Biosens. Bioelectron.*, 2019, **128**, 129–136.
26 X. Jin, G. Fang, M. Pan, Y. Yang, X. Bai and S. Wang, *Biosens. Bioelectron.*, 2018, **102**, 357–364.
27 Y. Gu, Z. Jiang, D. Ren, Y. Shang, Y. Hu and L. Yi, *Sens. Actuators, B*, 2021, 337.
28 P. Lei, R. An, S. Yao, Q. Wang, L. Dong, X. Xu, K. Du, J. Feng and H. Zhang, *Adv. Mater.*, 2017, **29**, 1700505.
29 L. Wang, Y. Liu, J. He, M. J. Hourwitz, Y. Yang, J. T. Fourkas, X. Han and Z. Nie, *Small*, 2015, **11**, 3762–3767.
30 L.-L. Li, J. Ji, R. Fei, C.-Z. Wang, Q. Lu, J.-R. Zhang, L.-P. Jiang and J.-J. Zhu, *Adv. Funct. Mater.*, 2012, **22**, 2971–2979.
31 D. Pan, Z. Fang, E. Yang, Z. Ning, Q. Zhou, K. Chen, Y. Zheng, Y. Zhang and Y. Shen, *Angew. Chem., Int. Ed.*, 2020, **59**, 16747–16754.
32 F.-N. Xiao, M. Wang, F.-B. Wang and X.-H. Xia, *Small*, 2014, **10**, 706–716.
33 L. Zhao, J. Li, Y. Liu, Y. Wei, J. Zhang, J. Zhang, Q. Xia, Q. Zhang, W. Zhao and X. Chen, *Sens. Actuators, B*, 2016, **232**, 484–491.